OXFORD

Journal of Geophysics and Engineering

Journal of Geophysics and Engineering (2020) **17**, 906–913 doi:10.1093/jge/gxaa051

Seismic shot-encoding schemes for waveform inversion

Edwin Fagua Duarte[1], **Carlos A.N. da Costa**[1], **João M. de Araújo**[1], **Yanghua Wang**[2] and **Ying Rao**[3,*]

[1] Department of Theoretical and Experimental Physics, Universidade Federal do Rio Grande do Norte, Natal, Brazil
[2] Centre for Reservoir Geophysics, Resource Geophysics Academy, Imperial College London, London SW7 2BP, UK
[3] State Key Laboratory of Petroleum Resources and Prospecting, College of Geophysics, China University of Petroleum (Beijing), Beijing 102249, China

*Corresponding author: Ying Rao. Email: raoying@cup.edu.cn

Received 11 May 2020, revised 7 July 2020
Accepted for publication 24 July 2020

Abstract

A shot-encoding technique can be used in seismic waveform inversion to significantly reduce the computational cost by reducing the number of seismic simulations in the inversion procedure. Here we developed two alternative shot-encoding schemes to perform simultaneous-sources waveform inversion. The first scheme (I) encodes shot gathers with random-phase rotations applied to seismic traces. The second scheme (II) encodes shot gathers with random static time shifts. The well-known polarity encoding scheme (III) is just a special case of the random-phase rotation scheme. The second scheme is a variation of the conventional static shift encoding (IV), but the static time shifts in the second scheme are limited to one period of the dominant frequency. All encoded shot gathers are added up into a single super-shot gather for seismic waveform inversion. We perform the time-domain waveform inversion, using these shot-encoding schemes in conjunction with a restarted L-BFGS algorithm in the iterative inversion. The effectiveness and efficiency analyses demonstrate that the two shot-encoding schemes (I and II) proposed in this paper may improve the convergence of the iterative inversion, reduce the crosstalk effect among shots and consequently produce a subsurface velocity model with a high resolution.

Keywords: FWI, seismic tomography, shot encoding, simultaneous-shot scheme, waveform tomography

1. Introduction

Seismic waveform tomography, also known as full waveform inversion (FWI), is an inversion technique for reconstructing wave velocities and other physical properties based on the field seismic waveforms (Tarantola 2004; Virieux & Operto 2009). This inversion technique is formulated as an optimisation problem, which minimises the data misfit between the simulated seismic waveforms and the field seismic waveforms. Most of the optimisation methods are iterative methods based on the gradient of the data misfit (Wang 2016). The most-used technique for gradient calculation is the adjoint-state method, in which the simulated forward wavefield is correlated with the backpropagation wavefield of the data misfit (Ren *et al.* 2013). The operation for the gradient calculation is performed for each shot gather independently, and thus the amount of computational time spent on the gradient calculation is linearly proportional to the number of shots in the seismic survey.

© The Author(s) 2020. Published by Oxford University Press on behalf of the Sinopec Geophysical Research Institute. This is an Open Access article distributed under the terms of the Creative Commons Attribution License (http://creativecommons.org/licenses/by/4.0/), which permits unrestricted reuse, distribution, and reproduction in any medium, provided the original work is properly cited.

The gradient calculation for a single shot gather requires two wavefield simulations. One simulation is the forward wave propagation started from the source point, and another simulation is for the backward propagation of the data misfit. For a seismic survey with N_S shots, it is necessary to perform wave simulations $2N_S$ times to build the gradient vector. Therefore, the standard waveform inversion is a computationally expensive problem, mainly because it requires a lot of computational resources and time for the gradient calculation in a realistic sized application (Krebs *et al.* 2009; Wang & Rao 2009; Ben-Hadj-Ali *et al.* 2011; da Costa *et al.* 2018).

One strategy to accelerate the gradient calculation is to use a simultaneous-shot scheme in which all shots are added up to form a super shot and this super shot is used to perform forward and backward propagation (Krebs *et al.* 2009; Rao & Wang 2017). Using the simultaneous-shot scheme, the number of wavefield simulations required at each iteration of the inversion is reduced to just two. In reality, often only one super shot is enough to calculate the gradient (Castellanos *et al.* 2014) if the group of shots shares the same set of receivers such as OBC/OBN acquisitions. Nevertheless, there are strategies to deal with shots with different sets of receivers (Choi & Alkhalifah 2012; Son *et al.* 2014).

However, a drawback of the simultaneous-shot scheme for the gradient calculation is the crosstalk effect that arises from the wavefield correlation between the forward and backward propagations coming from different shots. Romero *et al.* (2000) and Krebs *et al.* (2009) suggest use a shot-encoding scheme to mitigate the crosstalk effect in migration and inversion, respectively. In the shot-encoded waveform inversion, it applies a mathematical transformation to the amplitudes of each shot before summing them up.

One of the shot-encoding schemes in waveform inversion is the random-polarity encoding (Krebs *et al.* 2009), which multiplies a shot gather by a random number either $+1$ or -1. Another shot-encoding scheme is applying a static shift to each shot chosen randomly (Schuster *et al.* 2011). In addition, strategies exist to apply the codes for each shot; for example, using a multiscale strategy (Wang 2016), creating several super shots instead of one (Castellanos *et al.* 2014) or combining encoding schemes with deblurring filters in order to mitigate the crosstalk effect in waveform inversion.

In this paper, we propose two alternative shot-encoding schemes. The first scheme (I) applies random-phase rotations to seismic traces and their Hilbert transforms. The second scheme (II) applies random static time shifts to seismic traces. The conventional random-polarity encoding scheme (III) is a special case of the first scheme. The conventional static shift scheme (IV) (Schuster *et al.* 2011) is a general case of the second scheme. But the second scheme (II) limits the static values to one period of the dominant frequency of the observed seismic data. We will demonstrate that in this way we can improve the result of seismic waveform inversion. We use the random-polarity encoding scheme (III) as a benchmark to compare to other schemes (I, II and IV).

In order to further mitigate the crosstalk effect through the iterations, we combine the shot-encoding strategies with a restarted L-BFGS algorithm proposed by Rao & Wang (2017). If comparing this restarted algorithm to the previous works such as Castellanos *et al.* (2014), Rao & Wang's restarted algorithm calculates the gradient difference in L-BFGS based on the secant equation, which represents the gradient differential rather than the gradient difference. Using the gradient differential will improve the accuracy and, in turn, the stability of convergence of the iterative inversion. The central idea of a restarted algorithm is to effectively increase the randomness in an accumulative way by re-setting the codes every few iterations.

2. Two shot-encoding schemes

We develop two shot-encoding schemes. One is the random-phase rotation scheme (I), and the other is the random static time-shifting limited to one period of the dominant frequency (II). We compare these two schemes to the random-polarity encoding scheme (III) and the conventional static shift scheme (IV).

The random-phase rotation scheme (I) is applied for the first time to seismic waveform inversion. To illustrate the effect of shot-encoding schemes, we show in figure 1a a super shot gather formed from a series of shot gathers, each of which only collects 20 near-offset (the source-receiver distance) traces. Figures 1b–1d show the super shot gather after random-polarity change, random-phase rotation and random static time shift. The waveform change of a shot gather is equivalent to the change of the associated source signature.

In the random-phase rotation scheme (II), all seismic traces within each shot gather are rotated with a random phase φ in the interval $0 \leq \varphi \leq \pi$(figure 1c). The phase rotation of a time series $x(t)$ is performed using a time-domain equation:

$$x_{\text{rot}}(t;\varphi) = x(t)\cos\varphi + H[x(t)]\sin\varphi, \tag{1}$$

where $H[x(t)]$ is the Hilbert transform of $x(t)$ (Barnes 2007). This random-phase rotation scheme with the extreme values of $\cos\varphi = \pm 1$ corresponds to the random-polarity encoding scheme (III). The value of phase is constant for all trace within a single shot gather but is randomly different for any other shot. After phase rotation, all traces at the same position but from different shot gathers are stacked so as to create a super-shot gather of the observed seismic data. In the wavefield simulations that are needed in the waveform inversion, the source signatures are phase rotated by the chosen phase angle and then deployed at the shot positions.

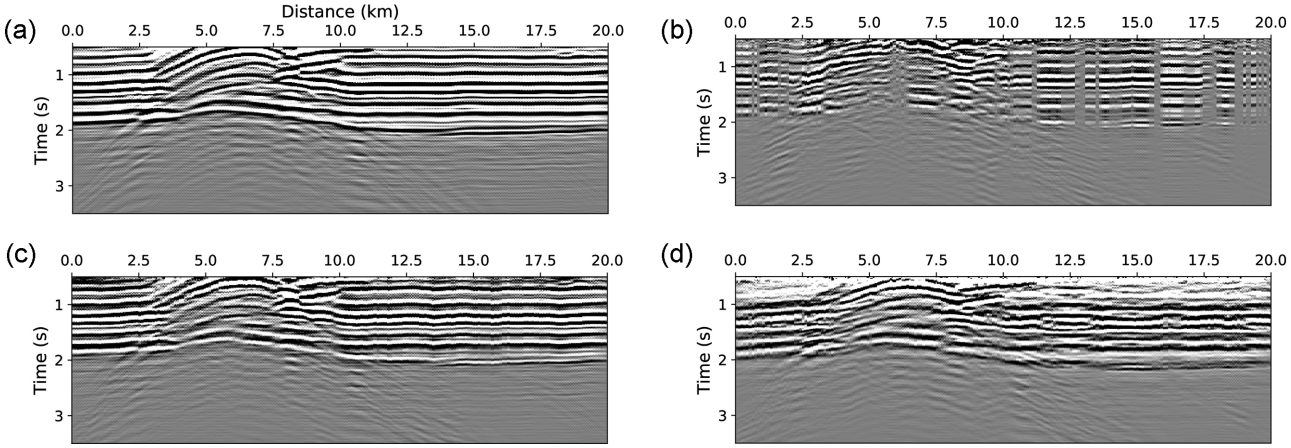


Figure 1. (a) The super shot gather formed from seismic shot gathers. (b) The super shot gather with random-polarity encoding scheme (III). (c) The super shot gather with random-phase-rotation encoding scheme (I). (d) The super shot gather with random static time-shift encoding (II). Each trace in the super shot gather is the stack of all traces at the same position but from different shots.

In the static time-shift scheme (II), a randomly assigned time shift is applied to all traces of an individual shot gather (figure 1d). The term static means that the time shift is applied to an entire seismic trace. The value of static time is a constant for all traces within a shot gather but is randomly different for each shot. In the wavefield simulation during the waveform inversion, the same static time shift is applied to the source signature at the corresponding shot position. This encoding strategy is used on the simultaneous-source acquisition (Stefani *et al.* 2007).

In the conventional static shift scheme (IV), the static Δs is a function the record length of data (Schuster *et al.* 2011). In this paper, the second scheme (II) limits the static Δs to one period of the dominant frequency of observed data. That is

$$0 \leq \Delta s \leq \frac{1}{f_0}, \tag{2}$$

where f_0 is the dominant frequency of the observed seismic data. We have found from our experiments that this constraint to the static values leads to a better result of seismic waveform inversion.

We note that both the phase-rotation encoding scheme (I) and the static time-shift encoding (II) are time-domain versions of the frequency-domain phase encoding scheme (Ben-Hadj-Ali *et al.* 2011; Castellanos *et al.* 2014), where the amplitudes of seismic traces in the frequency domain are multiplied by a pure phase term $e^{i\theta}$ with a randomly chosen phase θ. To show this assertion, we noticed that a time-shifted function satisfies the following Fourier transform property (Bracewell 1999)

$$F[x(t-\Delta s)](\omega) = e^{i\omega\Delta s} F[x(t)](\omega), \tag{3}$$

where $F[x(t)](\omega)$ is the Fourier transform of $x(t)$. In the same way the phase rotation of equation (1) also has a frequency-domain version as (Purves 2014)

$$F[x_{rot}(t;\varphi)](\omega) = F[\mathrm{x}(t)](\omega) \cdot \begin{cases} e^{-i\varphi}, & \omega < 0, \\ 0, & \omega = 0, \\ e^{+i\varphi}, & \omega > 0. \end{cases} \tag{4}$$

Therefore, both the random-phase rotation scheme (I) and the random static time-shift scheme (II) are a multiplication of seismic amplitudes by an imaginary exponential with random phase and, consequently, are the time-domain versions of the frequency-domain phase encoding scheme.

Figure 2a displays unmigrated constant-offset profile, in which each trace is collected from a shot gather and is annotated by its mid-point (of a source-receiver pair) coordinate. Figures 2b–2d show the profiles after random-polarity change, random-phase rotation and random static time shift. Each trace in these constant-offset profiles represents the waveform changes of all seismic traces within a shot gather after any shot encoding.

3. Waveform inversion with the restarted L-BFGS algorithm

The shot-encoding schemes can help to mitigate the crosstalk effect in a simultaneous-source waveform inversion to some extent. But it is necessary to change the shot codification throughout the inversion iterations (Krebs *et al.* 2009). Rao & Wang (2017) proposed a restarted L-BFGS algorithm for an iterative updating in the inversion, which can increase the effective randomness of a shot-encoding scheme and, thus, eventually achieve a complete crosstalk mitigation. This algorithm is different from the strategy of Krebs *et al.* (2009), where the shot codification changed at every iteration. Rao–Wang's restarted L-BFGS algorithm keeps the initial codification for m iterations, changes the codification every iteration

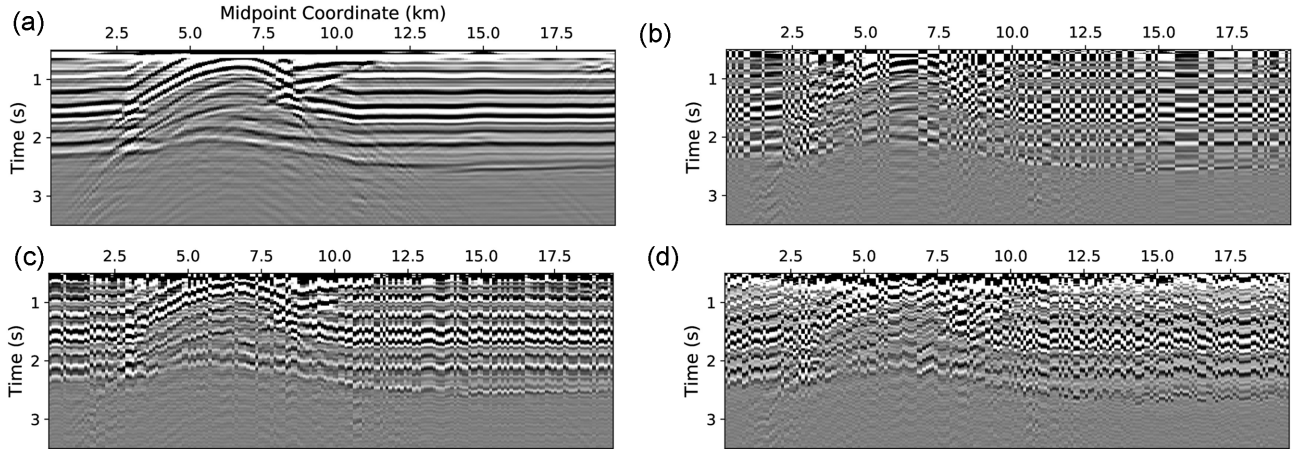


Figure 2. (a) Prestack seismic profiles in which the constant offset (the source-receiver distance) is 500 m. (b) The constant-offset profile with random-polarity encoding scheme (III). (c) The constant-offset profile with random-phase-rotation encoding scheme (I). (d) The constant-offset profile with random static time-shift encoding (II).

of the following iterations until the reach $\ell(>m)$ iterations and then restarts the L-BFGS calculation. The waveform inversion repeats this restarted procedure until reaching convergence.

There are variant schemes similar to this restarted L-BFGS algorithm, such as Guitton & Diaz (2012), Castellanos *et al.* (2014), Rao & Wang (2017), Rao *et al.* (2019). In this paper, we choose Rao–Wang's restarted L-BFGS algorithm, because this algorithm outperforms other similar schemes, as shown by Rao *et al.* (2019).

In the shot-encoded waveform inversion, the objective function is defined by the data misfit between simulated waveforms and observed waveforms as

$$J = \frac{1}{2}\left\| P - \sum_{i=1}^{N_S} {p_{\text{obs}}}^{(i)} \right\|_2^2, \tag{5}$$

where P is the simulated super shot, $\sum_{i=1}^{N_S} {p_{\text{obs}}}^{(i)}$ is the super gather of encoded field seismic data and $\|\cdot\|_2$ is the L_2 norm. The simulated super shot P is the solution of the following wave equation:

$$\nabla^2 P - \frac{1}{c^2(\vec{x})}\frac{\partial^2 P}{\partial t^2} = \sum_{i=1}^{N_S} e_i(t) \otimes s_i(t), \tag{6}$$

where $\vec{x}$ is the spatial coordinate, and $e_i \otimes s_i(t)$ is the shot-encoding operation.

The gradient vector of the objective function (5) is calculated as

$$\nabla J = -\int_0^T R(\vec{x}, t)\frac{\partial^2 P(\vec{x}, t)}{\partial t^2}\mathrm{d}t, \tag{7}$$

where R is the back-propagated wavefield and is calculated by solving equation (8),

$$\nabla^2 R - \frac{1}{c^2(\vec{x})}\frac{\partial^2 R}{\partial t^2} = P(T-t) - \sum_{i=1}^{N_S} e_i(T-t) \otimes d_i(T-t). \tag{8}$$

The $T - t$ in the argument on the source term means that the wavefield is time reversed. Taking linearity of the wave equation, the gradient vector of equation (7) can be expressed as

$$\begin{aligned}\nabla J = &-\sum_{i=1}^{N_S}\int_0^T e_i(T-t) \otimes R_i(T-t)\frac{\partial^2 e_i \otimes P_i(t)}{\partial t^2}\mathrm{d}t \\ &-\sum_{i\neq j}^{N_S}\int_0^T e_i(T-t) \otimes R_i(T-t)\frac{\partial^2 e_j \otimes P_j(t)}{\partial t^2}\mathrm{d}t.\end{aligned} \tag{9}$$

The first term is the correlations between the forward and backward propagation of the same shot i, whereas the second term is the crosstalk effect between shots i and j. For any shot-encoding strategy to work properly, the first term should be exactly the gradient vector in the conventional waveform inversion as

$$\nabla J_{\text{conv}} = -\sum_{i=1}^{N_S}\int_0^T R_i(\vec{x}, t)\frac{\partial^2 P_i(\vec{x}, t)}{\partial t^2}\mathrm{d}t, \tag{10}$$

where $P_i(\vec{x}, t)$ and $R_i(\vec{x}, t)$ are the forward and backward wavefields of shot i.

To show that the shot-encoding schemes satisfy this requirement, we can apply the Parseval relation to the first term

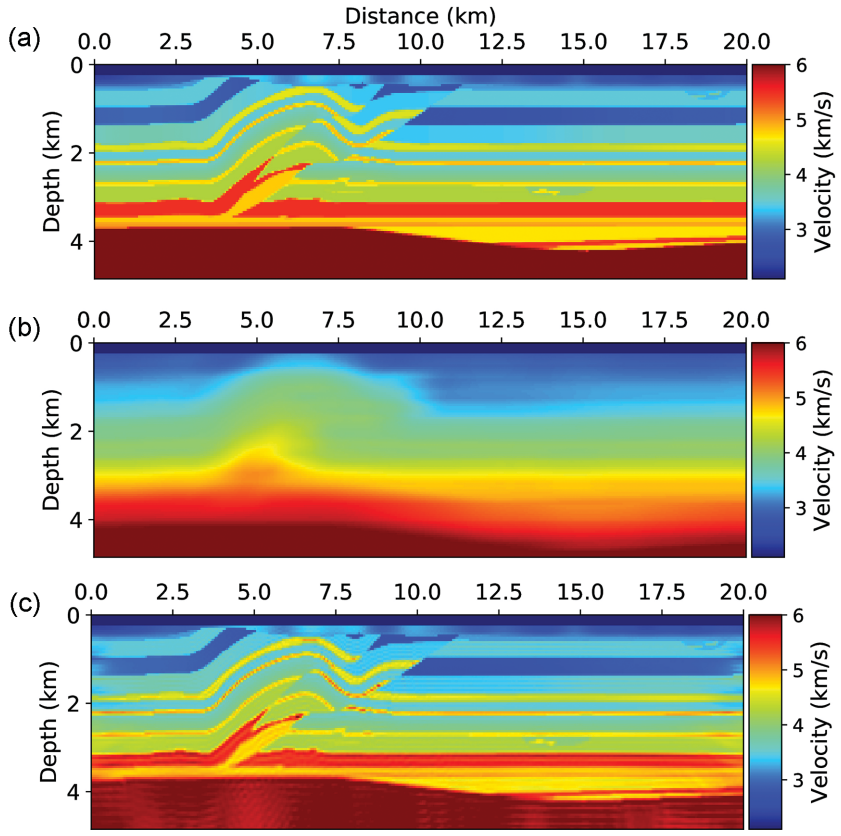


Figure 3. (a) The SEG/EAGE overthrust velocity model. (b) A smoothed model that is used as the initial model for seismic waveform inversion. (c) The inverted model from the conventional waveform inversion without shot encoding after 150 iterations.

of equation (9) and obtain the relation

$$\nabla J_{\text{conv}} = \sum_{i=1}^{N_S} \int \omega^2 \hat{e}_i^*(\omega)\hat{e}_i(\omega)\hat{R}_i^*(\vec{x},\omega)\hat{P}_i(\vec{x},\omega)\mathrm{d}\omega, \tag{11}$$

where $\hat{e}_i(\omega)$ is the frequency-domain encoding operator, and $\hat{e}_i^*(\omega)$ is the frequency-domain reverse-time encoding operator. All three shot-encoding schemes satisfy that $\hat{e}_i^*(\omega)\hat{e}_i(\omega) = 1$. In the same way, the second term of equation (9) satisfies the requirement $\hat{e}_i^*(\omega)\hat{e}_j(\omega) = 0$. The crosstalk term approaches zero because of the variation of shot-encoding throughout the iterations. We will prove in the next section that the shot-encoded waveform inversion can produce the same result as that obtained from the conventional waveform inversion, but with a remarkable high efficiency.

4. The effectiveness of shot-encoded waveform inversion

For demonstrating the effectiveness, seismic waveform inversion is performed in the time domain and full waveform data are used as the input to the inversion, rather than inverting frequency-banded data sequentially for field seismic data (Wang 2011).

The SEG/EAGE Overthrust velocity model (figure 3a) is used to demonstrate the effectiveness of waveform inversion with different shot-encoding schemes. The 2D model consists of 401 × 98 cells and the cell size is 50 m. Therefore, the model dimension was 20 × 4.85 km^2. The first five rows have a constant-velocity value of 2.1 km s^{-1}. This constant-velocity layer is also set as a known layer in the initial model, so that the gradient is zero in the area next to the source and receiver positions.

We use a finite-difference method to solve the acoustic wave equation (equations (6) and (8)) and apply an absorbing boundary layer to all sides of the model. We use 30-cell CPML method for the boundary absorbing layer (Liu & Sen 2018; He *et al.* 2020). There are 201 shots disposed at the surface. The source signature is a Ricker wavelet with the peak frequency of 6 Hz (Wang 2015a, 2015b). One receiver for each column of the model is positioned at the surface. Each trace has 1500 samples in time with a sample interval of 4 ms.

A synthetic data set generated from the SEG/EAGE Overthrust velocity model (figure 3a) is used as the observed seismic data for waveform inversion. We implement the inversion iteratively and set a smooth version of the true model to be the initial model (figure 3b). The restarted L-BFGS algorithm has two parameters: ℓ, the number of iterations of each segment before re-starting the calculation and m, the number

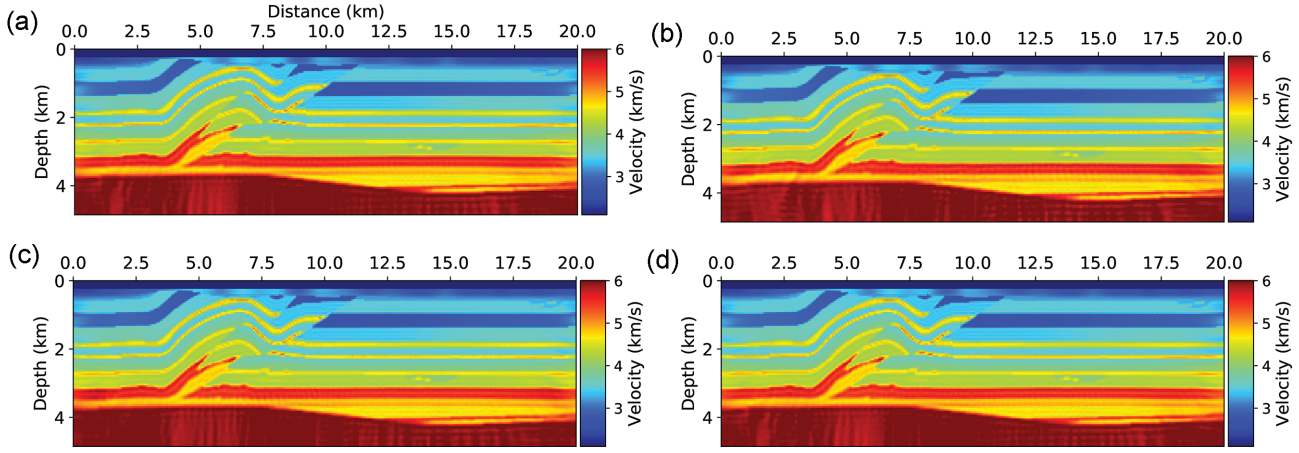


Figure 4. Seismic waveform inversion with different shot-encoding schemes. (a) The inverted model from the waveform inversion with the random-polarity encoding (III), after 775 iterations. (b) The inverted model from the waveform inversion with the random-phase-rotation encoding (I), after 250 iterations. (c) The inverted model from the waveform inversion with the random static time-shift encoding (II), after 355 iterations. (d) The inverted model from the waveform inversion with the random static time-shift encoding with ten periods of dominant frequency (IV), after 690 iterations.

of iterations with re-encoding within a segment. For all inversions presented in this paper, we use $\ell = 5$ and $m = 2$, as the same as those used in the original paper (Rao & Wang 2017). Figure 3c is the result of the conventional waveform inversion without shot encoding. The inversion procedure is performed on 201 shots sequentially and implemented for 150 iterations for each shot gather.

The result obtained from this conventional waveform inversion can be used as a benchmark. Figure 4a is the result of waveform inversion with the random-polarity scheme (III), and figures 4b–4d show the results of waveform inversion with the random-phase-rotation scheme (I), the random static time-shift scheme (II) and random static time-shift scheme with ten periods of dominant frequency (IV), respectively. The stopping criterion is set as

$$J^{(k)}/J^{(0)} < \varepsilon^2, \tag{12}$$

where J_k is the misfit value where the iteration stop, J_0 is the misfit for the initial velocity, ε^2 is a threshold value to stop the iteration and $\varepsilon = 0.03$ is used in the numerical experiments presented in this paper.

As observed in figure 4, all encoding strategies show a similar quality to the conventional FWI. The inversion with the random-polarity encoding (III) takes 775 iterations to reach the stopping criterion and is the slowest among the encoding strategies. The inversions with either the proposed random-phase-rotation encoding (I) or the random shift encoding (III) converge faster than the inversion with the polarity encoding, and need less than a half of the iterations than the inversion with the polarity encoding. The inversion with scheme IV spends around two times the number of iterations in the inversion with scheme II. This fact supports the idea of limiting the range of the static to one period of dominant frequency.

Figure 5a shows the data misfit versus the iteration number for all different schemes (I, II, III and IV). All shot-encoded inversions have a slow decay of the data misfit than the conventional waveform inversion, if considering only the number of iterations. However, figure 5b indicates that the conventional waveform inversion without shot encoding needs number of wavefield simulations two magnitude orders more than any shot-encoded waveform inversions need.

Figure 5 clearly indicates that the inversion using the random-polarity scheme (III) and the inversion using the conventional static shift scheme with ten periods of dominant period (IV) have similar convergence rates. However, the inversions with two schemes proposed in this paper (I and II) show even faster convergence rates than those the two schemes mentioned above.

In these inversions, the step length for updating is fixed to unity for each iteration. An optimum step-length calculation needs a proper line search, and the linear search is affected by the crosstalk effect present on the gradient. However, as explained in Nocedal & Wright (2006), the secant equation for the L-BFGS method scales well enough the gradient and thus the calculation of step length can be avoided in most cases.

The correlation coefficient calculated position by position is a quantitative comparison between a waveform inversion result and the true velocity model (Gao & Wang 2020). The localised correlation coefficient at position (i, j) is calculated by

$$c_{i,j} = \frac{\sum A \cdot B}{\max(\sum A \cdot A, \sum B \cdot B)}, \tag{13}$$

where A and B are 5×5 matrices centered on the target position of the true model and an inversion result, and the dot operation represents a pointwise matrix multiplication. The localised correlation-coefficient images indicate that (i)

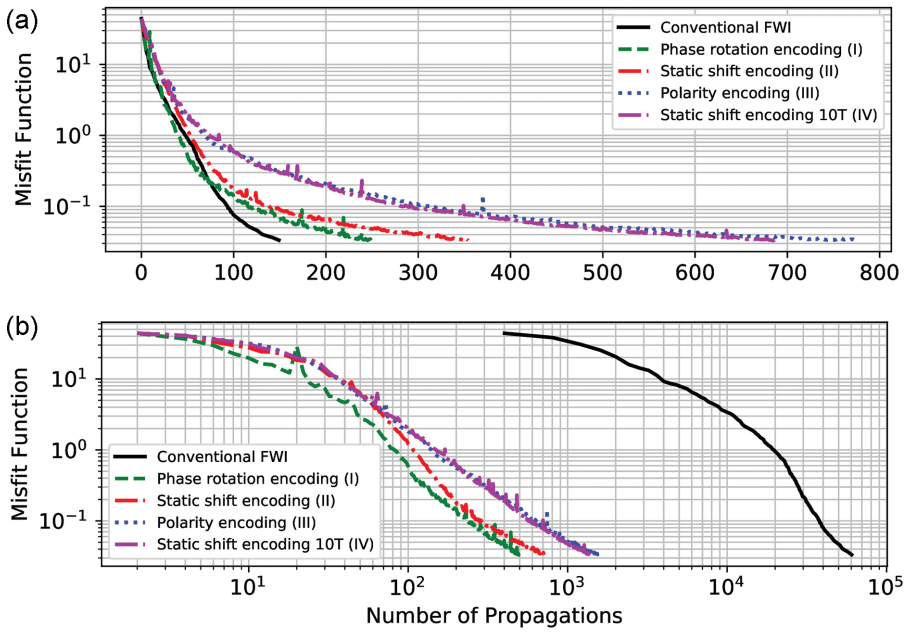


Figure 5. The convergence rates of seismic waveform inversions with various shot-encoding schemes (I, II, III and IV) and the conventional waveform inversion without shot encoding. (a) Data misfit versus the iteration number. (b) Data misfit versus the number of wavefield simulations.

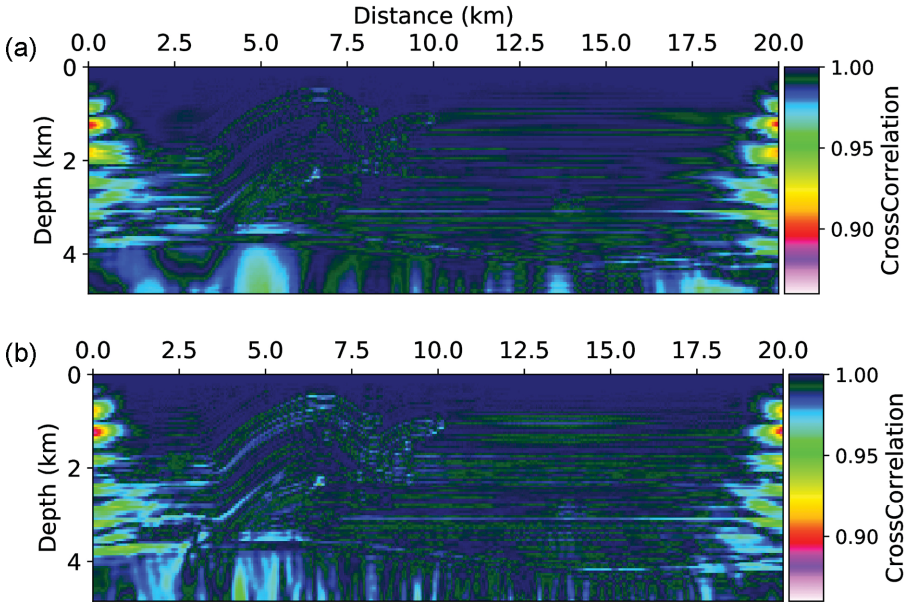


Figure 6. (a) Localised correlation-coefficient image between the true model and the inverted model from the conventional waveform inversion without shot encoding. (b) Localised correlation-coefficient image between the true model and the inverted model from the waveform inversion using the random-phase rotation scheme (I).

there is no any remarkable difference between the model from the conventional waveform inversion without shot encoding (figure 6a) and the model from any shot-encoded waveform inversions (figure 6b), and (ii) there is no any remarkable difference among all three shot-encoded waveform inversions. Therefore, figure 6 displays only one of these correlation-coefficient images (figure 6b).

In fact, figure 6 clearly demonstrates the effectiveness of seismic waveform inversion when the inversion employs seismic reflection data. It is referred to as the resolving power of the waveform inversion (Rao *et al.* 2006). One of the difficulties in seismic reflection waveform inversion is the reconstruction of the deep part of the subsurface model. We adopt the depth-dependent weighting scheme for the model update, closely following the strategy proposed in Wang & Rao (2009), to improve the reconstruction of deep structures. Figure 6 indicates an excellent recovery of the deep part velocity model from the

seismic reflection waveform inversion with or without shot encoding.

5. Conclusions

We have proposed the random-phase-rotation scheme (I) and the random static time-shift scheme constrained to one period of dominant frequency (II), for seismic waveform inversion, and compared them with the inversions using the random-polarity scheme (III) and the conventional static shift scheme defined as a function the record length of data (IV). We have demonstrated that all shot-encoding schemes, in conjunction with the restarted L-BFGS algorithm, can mitigate the crosstalk effect in the waveform inversion. Waveform inversion with any of these schemes produces a similar result to that obtained from the conventional waveform inversion without shot encoding. But the waveform inversion with any shot-encoding scheme has a remarkable efficiency in computation.

Among those four shot-encoding schemes, waveform inversion with two shot-encoding schemes proposed in this paper (I and II) have a better convergence, if compared to the inversion with other two shot-encoding schemes (III and IV). However, the inversion experiments have indicated that waveform inversion method with any shot-encoding scheme can make an excellent recovery of the deep part velocity model with the same effectiveness as the conventional waveform inversion without shot encoding.

Acknowledgements

This work was supported in part by Shell Brasil through the 'New Methods for Full Waveform Inversion' project at Universidade Federal do Rio Grande do Norte and the strategic importance of the support given by ANP through the R&D levy regulation, and in part by the Natural Science Foundation of China (grant nos. 41974118 and U19B6003) and Science Foundation of China University of Petroleum (Beijing) (grant no. 2462018BJC001). Authors would like to thank Jorge Lopez from Shell for the careful reading and comments on the manuscript.

Conflict of interest statement. None declared.

References

Barnes, A. E., 2007. A tutorial on complex seismic trace analysis, *Geophysics*, **72**, W33–W43.

Ben-Hadj-Ali, H., Operto, S. & Virieux, J., 2011. An efficient frequency domain full waveform inversion method using simultaneous encoded sources, *Geophysics*, **76**, R109–R124.

Bracewell, R. N., 1999. *The Fourier Transform and Its Applications*, McGraw-Hill.

Castellanos, C., Metivier, L., Operto, S., Brossier, R. & Virieux, J., 2014. Fast full waveform inversion with source encoding and second-order optimization methods, *Geophysical Journal International*, **200**, 720–744.

Choi, Y. & Alkhalifah, T., 2012. Application of multi-source waveform inversion to marine streamer data using the global correlation norm, *Geophysical Prospecting*, **60**, 748–758.

da Costa, C. A. N., Costa, J. C., Medeiros, W. E., Verschuur, D. J. & Soni, A. K., 2018. Target-level waveform inversion: a prospective application of the convolution-type representation for the acoustic wavefield, *Geophysical Prospecting*, **67**, 69–84.

Gao, F. & Wang, Y., 2020. Radiation pattern analyses for seismic multiparameter inversion of HTI anisotropic media, *Journal of Geophysics and Engineering*, **17**, 65–75.

Guitton, A. & Diaz, E, 2012. Attenuating crosstalk noise with simultaneous source full waveform inversion, *Geophysical Prospecting*, **60**, 759–768.

He, Y., Chen, T. & Gao, J., 2020. Perfectly matched absorbing layer for modelling transient wave propagation in heterogeneous poroelastic media, *Journal of Geophysics and Engineering*, **17**, 18–34.

Krebs, J. R., Anderson, J. E., Hinkley, D., Neelamani, R., Lee, S., Baumstein, A. & Lacasse, M.-D., 2009. Fast full-wavefield seismic inversion using encoded sources, *Geophysics*, **74**(6), WCC177–WCC188.

Liu, Y. & Sen, M. K., 2018. An improved hybrid absorbing boundary condition for wave equation modelling, *Journal of Geophysics and Engineering*, **15**, 2602–2613.

Nocedal, J. & Wright, S. J., 2006. *Numerical Optimization*, Springer New York.

Purves, S., 2014. Phase and the Hilbert transform, *The Leading Edge*, **33**, 1164–1166.

Rao, Y. & Wang, Y., 2017. Seismic waveform tomography with shot encoding using a restarted L-BFGS algorithm, *Scientific Reports*, **7**, article no. 8494, pp. 9.

Rao, Y., Wang, Y. & Han, D., 2019. Seismic waveform tomography with simplified restarting scheme, *IEEE Geoscience and Remote Sensing Letters*, **16**, 135–139.

Rao, Y., Wang, Y. & Morgan, J. V., 2006. Crosshole seismic waveform tomography, II: resolution analysis, *Geophysical Journal International*, **166**, 1237–1248.

Ren, H., Wang, H. & Chen, S., 2013. Least-squares reverse time migration in frequency domain using the adjoint-state method, *Journal of Geophysics and Engineering*, **10**, article no. 035002, pp. 7.

Romero, L. A., Ghiglia, D. C., Ober, C. C. & Morton, S. A., 2000. Phase encoding of shot records in prestack migration, *Geophysics*, **65**, 426–436.

Schuster, G. T., Wang, X., Huang, Y., Dai, W. & Boonyasiriwat, C., 2011. Theory of multisource crosstalk reduction by phase-encoded statics, *Geophysical Journal International*, **184**, 1289–1303.

Son, W., Pyun, S., Shin, C. & Kim, H.-J., 2014. An algorithm adapting encoded simultaneous-source full-waveform inversion to marine-streamer acquisition data, *Geophysics*, **79**, R183–R193.

Stefani, J., Hampson, G. & Herkenhoff, E. F., 2007. Acquisition using simultaneous sources, in *Proceedings of the 69th EAGE Conference and Exhibition, paper no. B006*.

Tarantola, A., 2004. *Inverse Problem Theory and Methods for Model Parameter Estimation*. SIAM.

Virieux, J. & Operto, S., 2009. An overview of full-waveform inversion in exploration geophysics, *Geophysics*, **74**(6), WCC1–WCC26.

Wang, Y. & Rao, Y., 2009. Reflection seismic waveform tomography, *Journal of Geophysical Research*, **114**(B9), article no. B03304, pp. 12.

Wang, Y., 2011. Seismic waveform modeling and tomography, *Encyclopaedia of Solid Earth Geophysics*, Springer Verlag, pp. 1290–1301.

Wang, Y., 2015a. Frequencies of the Ricker wavelet, *Geophysics*, **81**, A31–A37.

Wang, Y., 2015b. The Ricker wavelet and the Lambert *W* function, *Geophysical Journal International*, **200**, 111–115.

Wang, Y., 2016. *Seismic Inversion, Theory and Applications*. Wiley Blackwell, Oxford.